Supporting Information:

Switchable bulk photovoltaic effect in 2D room temperature ferroelectric $CuInP_2S_6$

Chengwei Liao,[1] Minglong Wang,[1] Yu-Jun Zhao[1,2,*]

[1]*Department of Physics, South China University of Technology, Guangzhou 510641, China*

[2]*Key Laboratory of Advanced Energy Storage Materials of Guangdong Province, South China University of Technology, Guangzhou 510641, China*

Contents

* Corresponding author.

E-mail address: zhaoyj@scut.edu.cn (Y.-J. Zhao).

1. Supplementary note: Formula derivation

Second-order nonlinear photoconductivity in the velocity gauge and length gauge. Under intense light irradiation, homogeneous systems with spatial inversion symmetry (*P*-symmetry) breaking exhibit even-order nonlinear optical responses. The bulk photovoltaic effect (BPVE) is a second-order nonlinear optical response, capable of generating a direct current under light field. The photocurrent can be derived using methods such as density matrix,[1,2] polarization operator,[3] and Feynman diagrams.[4] Employing the density matrix method and quadratic Kubo response theory, under the independent particle approximation, the expression for the second-order photocurrent density in the velocity gauge reads as follows:[1,2,5,6]

$$J_{bc}^{a} = -\frac{e^3}{\hbar^2\omega^2}\mathrm{Re}\left\{\sum_{m,n,l}^{\Omega=\pm\omega}\int_{BZ}\frac{d^3\boldsymbol{k}}{(2\pi)^3}f_{lm}\frac{v_{lm}^{b}}{\omega_{ml}-\Omega+i/\tau}\left(\frac{v_{mn}^{a}v_{nl}^{c}}{\omega_{mn}+i/\tau}-\frac{v_{mn}^{c}v_{nl}^{a}}{\omega_{nl}+i/\tau}\right)E_b(\Omega)E_c(-\Omega)\right\} \quad \text{(S1)}$$

where, *a* denotes the direction of the photocurrent, *b* and *c* denote the direction of the electric field of the incident light. This is a three-band model, the generalized photoconductivity $\chi_{bc}^{a}(0;\omega,-\omega)$ can be written as:

$$\chi_{bc}^{a}(0;\omega,-\omega) = -\frac{e^3}{\hbar^2\omega^2}\int_{BZ}\frac{d^3\boldsymbol{k}}{(2\pi)^3}\sum_{m,n,l}f_{lm}\frac{v_{lm}^{b}}{\omega_{ml}-\omega+i/\tau}\left(\frac{v_{mn}^{a}v_{nl}^{c}}{\omega_{mn}+i/\tau}-\frac{v_{mn}^{c}v_{nl}^{a}}{\omega_{nl}+i/\tau}\right) \quad \text{(S2)}$$

In systems where *P*-symmetry is broken while time-reversal symmetry (*T*-symmetry) is preserved, $Tv_{mn}(\boldsymbol{k}) = -v_{mn}^{*}(-\boldsymbol{k})$, where v_{mn}^{*} represents the complex conjugate of the velocity matrix. In the numerator part of χ_{bc}^{a}, $Tv_{mn}v_{nl}v_{lm} = -(v_{mn}v_{nl}v_{lm})^{*}$, implying that the real and imaginary parts of the numerator are odd and even functions in the ***k***-space, respectively. Hence, when integrating over the entire first Brillouin zone (BZ), only the imaginary part of the numerator contributes to the total photoconductivity, while the real part cancels out due to its opposite values at $\pm\boldsymbol{k}$ point. Under static constraints $\tau\to\infty$, according to the Sokhotski-Plemelj theorem $\lim_{x\to 0}\frac{1}{z\pm ix} = \mathcal{P}\frac{1}{z}\mp i\pi\delta(z)$ ($\mathcal{P}$ is the Cauchy principal value), the denominator part of the χ_{bc}^{a} can be expressed as:

$$D_1 = \lim_{1/\tau\to 0}\frac{1}{\omega_{ml}-\omega+i/\tau} = \mathcal{P}\frac{1}{\omega_{ml}-\omega} - i\pi\delta(\omega_{ml}-\omega) \quad \text{(S3)}$$

$$D_2 = \lim_{1/\tau\to 0}\frac{1}{\omega_{mn}+i/\tau} = \mathcal{P}\frac{1}{\omega_{mn}} - i\pi\delta(\omega_{mn}) \quad \text{(S4)}$$

$$D_3 = \lim_{1/\tau \to 0} \frac{1}{\omega_{nl} + i/\tau} = P\frac{1}{\omega_{nl}} - i\pi\delta(\omega_{nl}) \tag{S5}$$

Under linearly polarized light (LPL) illumination, inducing shift current (SC), the photoconductivity is denoted by σ. In LPL, there is no phase difference between the electric fields E_b and E_c. The numerator contributes only to the imaginary part, but the photocurrent must be a real quantity. Therefore, here we need to consider the imaginary part of the denominator:

$$\mathrm{Im}(D_1 D_2) = -\pi \frac{P}{\omega_{ml} - \omega}\delta(\omega_{mn}) - \pi\frac{P}{\omega_{mn}}\delta(\omega_{ml} - \omega) \tag{S6}$$

$$\mathrm{Im}(D_1 D_3) = -\pi \frac{P}{\omega_{ml} - \omega}\delta(\omega_{nl}) - \pi\frac{P}{\omega_{nl}}\delta(\omega_{ml} - \omega) \tag{S7}$$

the first term in $\mathrm{Im}(D_1 D_2)$ ($\mathrm{Im}(D_1 D_3)$) is symmetric under permutations of *m* and *n* (*n* and *l*). However, the imaginary part of the numerator $v_{mn} v_{nl} v_{lm}$ is antisymmetric under permutations, $v_{mn} = -v_{nm}$. Therefore, the first term cancels out and can be neglected. Hence, we focus on the imaginary part of the denominator's second term, yielding the σ_{bc}^{a} under the velocity gauge as:

$$\begin{aligned}
\sigma_{bc}^{a}(0;\omega,-\omega) &= -\frac{e^3}{\hbar^2\omega^2}\int_{BZ}\frac{d^3\boldsymbol{k}}{(2\pi)^3}\sum_{m,n,l} f_{lm}\frac{v_{lm}^{b}}{\omega_{ml} - \omega + i/\tau}\left(\frac{v_{mn}^{a}v_{nl}^{c}}{\omega_{mn} + i/\tau} - \frac{v_{mn}^{c}v_{nl}^{a}}{\omega_{nl} + i/\tau}\right) \\
&= -\frac{e^3}{\hbar^2\omega^2}\int_{BZ}\frac{d^3\boldsymbol{k}}{(2\pi)^3}\sum_{m,n,l} f_{lm}v_{lm}^{b}(-i\pi)\left(\frac{v_{mn}^{a}v_{nl}^{c}}{\omega_{mn}} - \frac{v_{mn}^{c}v_{nl}^{a}}{\omega_{nl}}\right)\delta(\omega_{ml} - \omega) \\
&= \frac{i\pi e^3}{\hbar^2}\int_{BZ}\frac{d^3\boldsymbol{k}}{(2\pi)^3}\sum_{m,n,l} f_{lm}\frac{v_{lm}^{b}}{\omega_{ml}^{2}}\left(\frac{v_{mn}^{a}v_{nl}^{c}}{\omega_{mn}} - \frac{v_{mn}^{c}v_{nl}^{a}}{\omega_{nl}}\right)\delta(\omega_{ml} - \omega)
\end{aligned} \tag{S8}$$

due to the energy selection law of the Dirac delta function $\delta(\omega_{ml} - \omega)$, so $\frac{1}{\omega^2} = \frac{1}{\omega_{ml}^2}$.

The relationship between the Berry connection r_{ml} and the velocity matrix v_{ml} is as follows:

$$r_{ml}^{a} = \frac{v_{ml}^{a}}{i\omega_{ml}} = -\frac{v_{lm}^{a}}{i\omega_{ml}} \ (m \neq l) \tag{S9}$$

sum rule,[7]

$$r_{lm;a}^{c} = \frac{i}{\omega_{lm}}\left[\frac{v_{lm}^{c}\Delta_{lm}^{a} + v_{lm}^{a}\Delta_{lm}^{c}}{\omega_{lm}} - w_{lm}^{ca} + \sum_{p \neq l,m}\left(\frac{v_{lp}^{c}v_{pm}^{a}}{\omega_{pm}} - \frac{v_{lp}^{a}v_{pm}^{c}}{\omega_{lp}}\right)\right] \ (m \neq l) \tag{S10}$$

where, $v_{ml}^{a} = \langle m|\frac{dH}{dk_a}|l\rangle$, $w_{lm}^{ca} = \langle l|\frac{d^2H}{dk_c dk_a}|m\rangle$, $\hbar\omega_{ml} = E_m - E_l$ is the energy difference between bands *m* and *l*, $\Delta_{lm}^{a} = v_{ll}^{a} - v_{mm}^{a}$ is the velocity difference. By utilizing the Berry connection and sum rule, the σ_{bc}^{a} can be transformed into an expression in the length gauge:

$$\sigma_{bc}^{a}(0;\omega,-\omega) = -\frac{i\pi e^3}{2\hbar^2}\int_{BZ}\frac{d^3\boldsymbol{k}}{(2\pi)^3}\sum_{m,l} f_{lm}\left(r_{ml}^{b}r_{lm;a}^{c} + r_{ml}^{c}r_{lm;a}^{b}\right)\delta(\omega_{ml} - \omega) \tag{S11}$$

where, $r^b_{ml} r^c_{lm;a} = I^{abc}_{ml}$ is the SC strength.

In order to have a more intuitive understanding of the physical mechanisms of SC, by simply transforming the SC σ^a_{bc} can be further written in a more popular and cleaner form:

$$\sigma^a_{bb}\left(0;\omega,-\omega\right) = -\frac{\pi e^3}{2\hbar^2}\int_{BZ}\frac{d^3\boldsymbol{k}}{\left(2\pi\right)^3}\sum_{m,l} f_{lm} R^{a,b}_{lm} \left|r^b_{ml}\right|^2 \delta\left(\omega_{ml}-\omega\right) \tag{S12}$$

where, $R^{a,b}_{lm}$ is the shift vector, $R^{a,b}_{lm} = \frac{\partial \phi^b_{lm}}{\partial k_a} - A^a_{ll} + A^a_{mm}$, $r^b_{lm} = \left|r^b_{lm}\right| e^{i\phi^b_{lm}}$, ϕ^b_{lm} is the phase factor of r^b_{lm}, r^a_{ml} and A^a_{ll} are interband and intraband Berry connections. $\left|r^b_{lm}\right|^2 = r^b_{lm} r^b_{ml}$ is the transition rate. For LPL, $b = c$. This constitutes a two-band model, by substituting l with n in the subscript, Eq. (S12) equals Eq. (6) in the main text.

Under circularly polarized light (CPL) illumination, inducing injection current (IC), also known as circular current or ballistic current, the photoconductivity is denoted by η. For CPL, the phase difference between the electric fields E_b and E_c is *i*. While only the imaginary part contributes to the photoconductivity in the numerator, the current must be a real. Therefore, we need to consider the real part of the denominator:

$$\mathrm{Re}\left(D_1 D_2\right) = \frac{P}{\omega_{mn}\left(\omega_{ml}-\omega\right)} + i\pi\delta\left(\omega_{mn}\right)\cdot i\pi\delta\left(\omega_{ml}-\omega\right) \tag{S13}$$

$$\mathrm{Re}\left(D_1 D_3\right) = \frac{P}{\omega_{nl}\left(\omega_{ml}-\omega\right)} + i\pi\delta\left(\omega_{nl}\right)\cdot i\pi\delta\left(\omega_{ml}-\omega\right) \tag{S14}$$

the contribution of the first term in $\mathrm{Re}\left(D_1 D_2\right)$ ($\mathrm{Re}\left(D_1 D_3\right)$) is much smaller than that of the second term. Hence, we neglect the first term here and only consider the second term. In the second term,

$$\frac{1}{\omega_{mn} - i/\tau} = \frac{P}{\omega_{mn}} + i\pi\delta\left(\omega_{mn}\right) \tag{S15}$$

when $m = n$, $\frac{1}{\omega_{mn}} \to \infty$, and the integral part $\frac{P}{\omega_{mn}} \to 0$ can be neglected. So,

$$i\pi\delta\left(\omega_{mn}\right) = \frac{1}{\omega_{mn} - i/\tau} = \frac{1}{-i/\tau} = i\tau \tag{S16}$$

when $n = l$, $i\pi\delta\left(\omega_{nl}\right) = i\tau$. The IC η^a_{bc} can be written as:

$$
\begin{aligned}
\eta_{bc}^{a}\left(0;\omega,-\omega\right) &= -\frac{e^{3}}{\hbar^{2}\omega^{2}}\int_{BZ}\frac{d^{3}\boldsymbol{k}}{\left(2\pi\right)^{3}}\sum_{m,n,l} f_{lm}\frac{v_{lm}^{b}}{\omega_{ml}-\omega+i/\tau}\left(\frac{v_{mn}^{a}v_{nl}^{c}}{\omega_{mn}+i/\tau}-\frac{v_{mn}^{c}v_{nl}^{a}}{\omega_{nl}+i/\tau}\right) \\
&= -\frac{e^{3}}{\hbar^{2}\omega^{2}}\int_{BZ}\frac{d^{3}\boldsymbol{k}}{\left(2\pi\right)^{3}}\sum_{m,n,l} f_{lm}v_{lm}^{b}\left(i\tau\right)\left(v_{mm}^{a}v_{ml}^{c}-v_{ml}^{c}v_{ll}^{a}\right)\cdot i\pi\delta\left(\omega_{ml}-\omega\right) \\
&= \tau\frac{\pi e^{3}}{\hbar^{2}}\int_{BZ}\frac{d^{3}\boldsymbol{k}}{\left(2\pi\right)^{3}}\sum_{m,n,l} f_{lm}\frac{v_{lm}^{b}v_{ml}^{c}}{\omega_{ml}^{2}}\left(v_{mm}^{a}-v_{ll}^{a}\right)\delta\left(\omega_{ml}-\omega\right) \\
&= \tau\frac{\pi e^{3}}{\hbar^{2}}\int_{BZ}\frac{d^{3}\boldsymbol{k}}{\left(2\pi\right)^{3}}\sum_{m,n,l} f_{lm}r_{ml}^{b}r_{lm}^{c}\left(v_{ll}^{a}-v_{mm}^{a}\right)\delta\left(\omega_{ml}-\omega\right)
\end{aligned}
\tag{S17}
$$

In CPL, the b and c directions are permutation antisymmetric, $bc \leftrightarrow -cb$, thus $r_{ml}^{b}r_{lm}^{c}=\frac{1}{2}\left(r_{ml}^{b}r_{lm}^{c}-r_{ml}^{c}r_{lm}^{b}\right)=\frac{1}{2}\left[r_{ml}^{b},r_{lm}^{c}\right]$. The η_{bc}^{a} can be transformed into an expression under the length gauge:

$$
\eta_{bc}^{a}\left(0;\omega,-\omega\right)=\tau\frac{\pi e^{3}}{2\hbar^{2}}\int_{BZ}\frac{d^{3}\boldsymbol{k}}{\left(2\pi\right)^{3}}\sum_{m,l} f_{lm}\Delta_{lm}^{a}\Omega_{ml}^{bc}\delta\left(\omega_{ml}-\omega\right) \tag{S18}
$$

where, $\Delta_{lm}^{a}=v_{ll}^{a}-v_{mm}^{a}$ is the velocity difference, $\Omega_{ml}^{bc}=\left[r_{ml}^{b},r_{lm}^{c}\right]=r_{ml}^{b}r_{lm}^{c}-r_{ml}^{c}r_{lm}^{b}$ is the Berry curvature, v_{ll}^{a} is the intraband velocity. Apart from a prefactor τ, replacing l with n in the subscript, Eq. (S18) equals Eq. (7) in the main text.

In fact, the photoconductivity under velocity gauge and length gauge is equal because they deal with the same physical effects. The difference lies in that Eq. (S2) can be used to handle cases where T-symmetry is either preserved or broken, while Eq. (S12) and Eq. (S18) require the system to maintain T-symmetry. In systems preserving T-symmetry, the symmetric real part and asymmetric imaginary part in Eq. (S2) respectively correspond to the photoconductivity under LPL and CPL illumination.

2. Supplementary tables

Table S1. The lattice parameters (Å) of CIPS, CIPSe, and CIPTe, as well as the energy differences (meV) between the FE, PE, and AFE phases. The *GS* denotes the ground state.

	FE1	FE2	PE	AFE	$\Delta E_1 = E_{PE} - E_{FE}$	$\Delta E_2 = E_{FE} - E_{AFE}$	*GS*
$CuInP_2S_6$	6.16	6.16	6.10	6.17	326.2	51.3	AFE
$CuInP_2Se_6$	6.50	6.50	6.45	6.52	161.9	26.7	AFE
$CuInP_2Te_6$	7.0	7.0	6.96	6.99	111.9	-14.2	FE

Table S2. The space group and point group of the FE, PE, and AFE phases of CIPS. The atomic structure is used to illustrate the presence of symmetry operations.

	FE1	FE2	PE	AFE
Space group	*P*3, (NO. 143)	*P*3, (NO. 143)	*P*312, (NO. 149)	$P2_1$, (NO. 4)
Point group	C_3	C_3	D_3	C_1

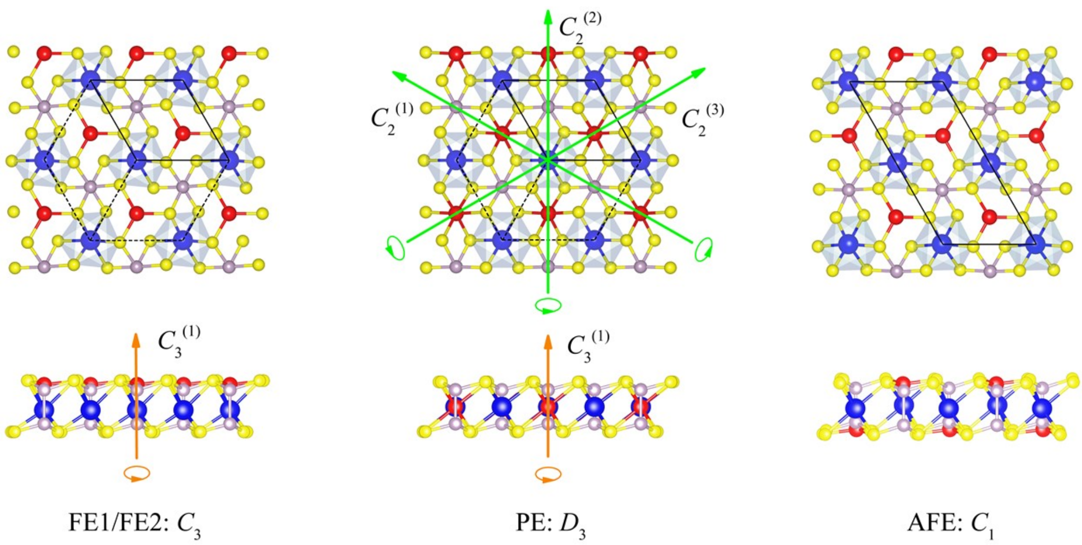

Table S3. The C_3, D_3, and C_1 point groups allowed second-order non-zero conductivity tensors.

Point group C_3			
$xxx = -xyy = -yyx = -yxy$,	$yyy = -yxx = -xxy = -xyx$,	$zxx = zyy$,	zzz
$xyz = -yxz$, $xzx = yzy$,	$yyz = xxz$, $yzx = -xzy$,	$zxy = -zyx$	

Point group D_3		
	$yyy = -yxx = -xxy = -xyx$	
$xyz = -yxz$,	$yzx = -xzy$,	$zxy = -zyx$

Point group C_1
All elements are independent and nonzero

Table S4. Transformation rules for the physical quantities in the SC and IC photoconductivity under the space inversion symmetry P and time-reversal symmetry T.

Quantity		**Space inversion *P***	**Time reversal *T***
Velocity	$v_{mn}(\boldsymbol{k})$	$-v_{mn}(-\boldsymbol{k})$	$-v^*_{mn}(-\boldsymbol{k})$
Berry Connection	$r_{mn}(\boldsymbol{k})$	$-r_{mn}(-\boldsymbol{k})$	$r^*_{mn}(-\boldsymbol{k})$
SC Strength	$I_{mn}(\boldsymbol{k})$	$-I_{mn}(-\boldsymbol{k})$	$-I^*_{mn}(-\boldsymbol{k})$
Transition Rate	$r_{nm}r_{mn}(\boldsymbol{k})$	$r_{nm}r_{mn}(-\boldsymbol{k})$	$r_{nm}r_{mn}(-\boldsymbol{k})$
Shift Vector	$R_{nm}(\boldsymbol{k})$	$-R_{nm}(-\boldsymbol{k})$	$R_{nm}(-\boldsymbol{k})$
Velocity Intraband	$v_{nn}(\boldsymbol{k})$	$-v_{nn}(-\boldsymbol{k})$	$-v_{nn}(-\boldsymbol{k})$
Velocity Difference	$\Delta_{mn}(\boldsymbol{k})$	$-\Delta_{mn}(-\boldsymbol{k})$	$-\Delta_{mn}(-\boldsymbol{k})$
Berry Curvature	$\Omega_{mn}(\boldsymbol{k})$	$\Omega_{mn}(-\boldsymbol{k})$	$-\Omega_{mn}(-\boldsymbol{k})$

3. Supplementary figures

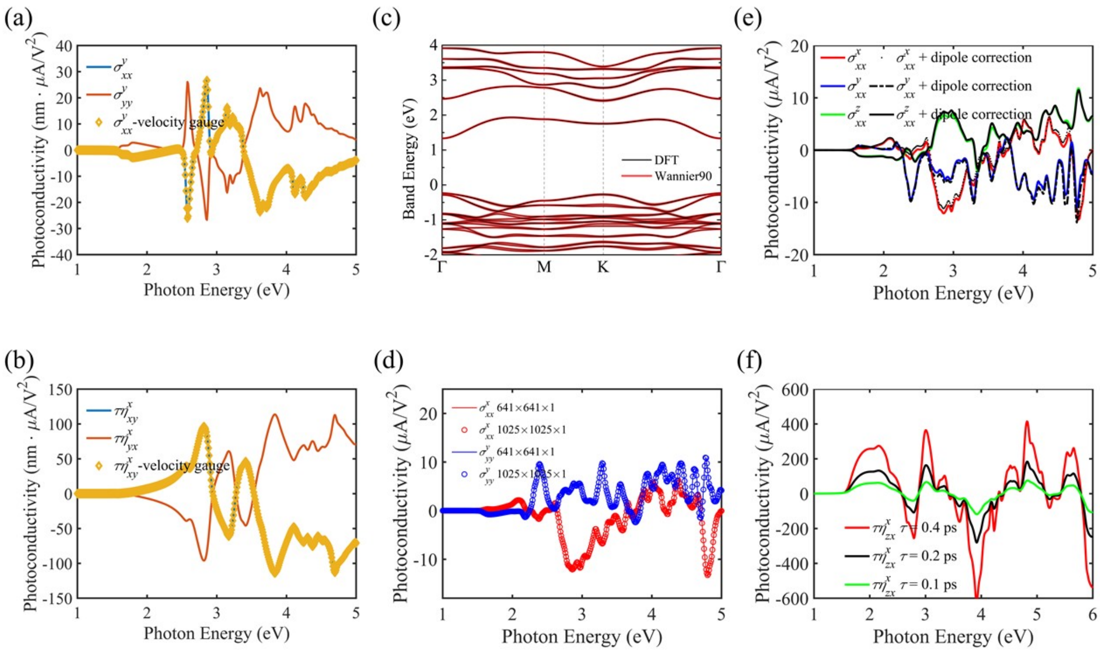

Figure S1. The SC (a) and IC (b) photoconductivities of $2H$-MoS_2, consistent with literature reported results.[5] The photoconductivity calculated using length gauges and velocity gauges are equivalent, denoted by lines and diamond markers, respectively. (c) Comparing the band structures of the FE1 phase of CIPS obtained from Wannier90 and DFT calculations. (d) The convergence test of k-point sampling density for photoconductivity calculations, confirming that the 641 × 641 × 1 k-mesh used in this paper has reached convergence. (e) The comparison between the photoconductivity calculations with and without dipole corrections shows that the dipole correction has a minimal effect on the photoconductivity. (f) The IC $\tau\eta^{x}_{zx}$ for carrier lifetimes (τ) of 0.1, 0.2, and 0.4 ps shows a positive correlation between the IC and the carrier lifetime.

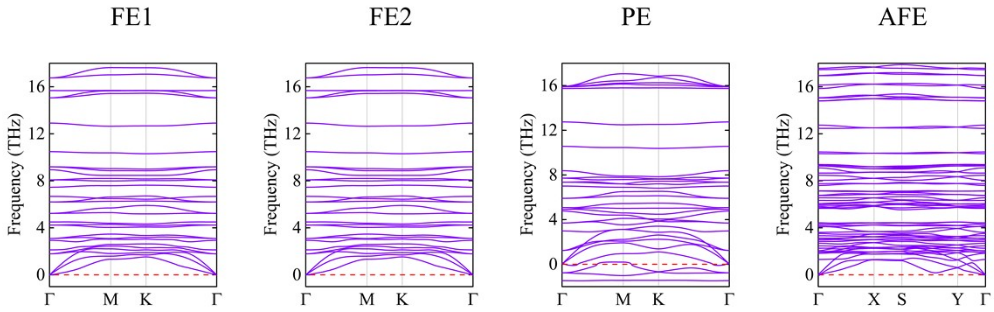

Figure S2. The phonon spectra of the the FE1, FE2, PE, and AFE phases of CIPS.

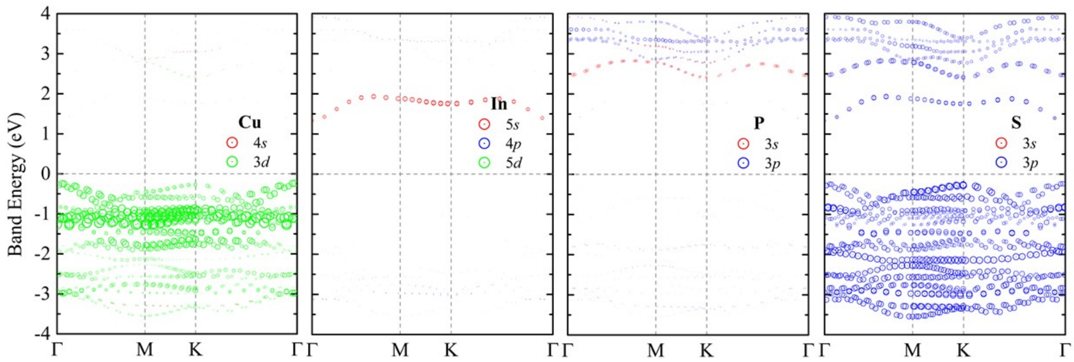

Figure S3. The projection band structure near the Fermi level for the FE1 phase of CIPS.

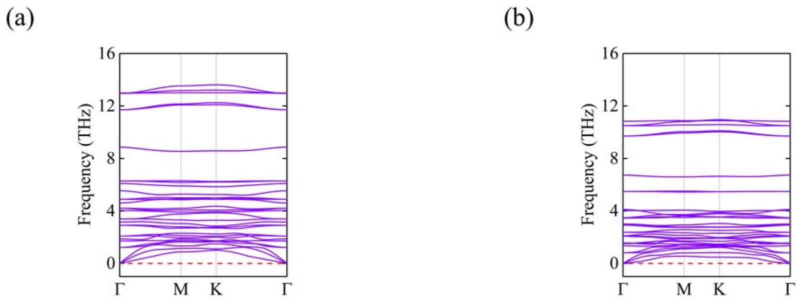

Figure S4. The phonon spectra of the FE phases of CIPSe (a) and CIPTe (b).

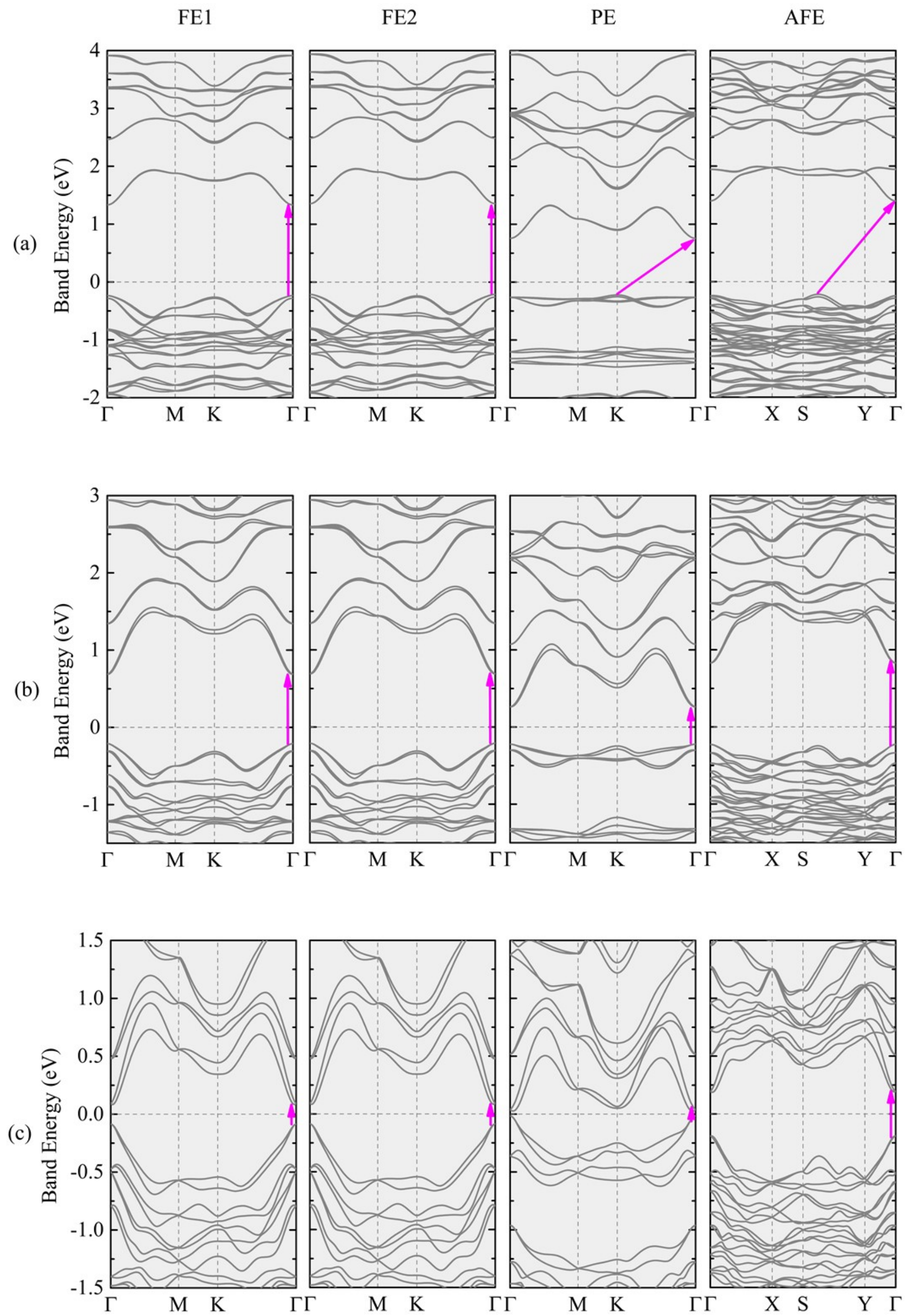

Figure S5. The band structures of the FE1, FE2, PE, and AFE phases for CIPS (a), CIPSe (b), and CIPTe (c).

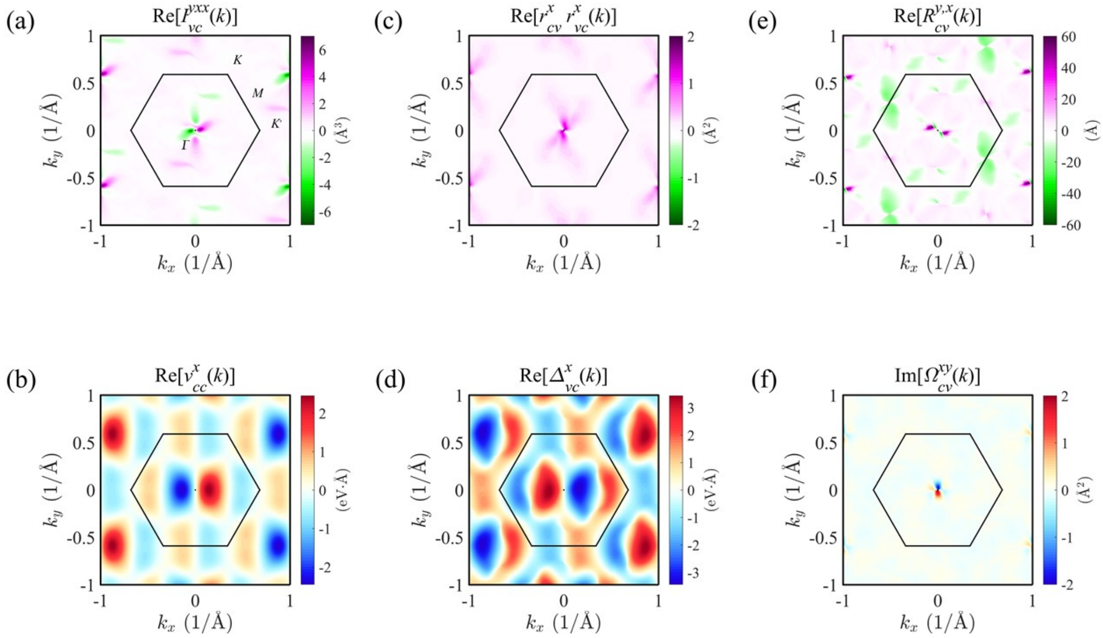

Figure S6. The distribution of physical quantities in ***k***-space. For SC σ_{xx}^{y}, (a) SC strength, (b) transition rate, (c) shift vector. For IC $\tau\eta_{xy}^{x}$, (d) velocity, (e) velocity difference, (f) Berry curvature. Here, we only consider the highest valence band *v* and the lowest conduction band *c*, which yields the same conclusions as considering all the bands.

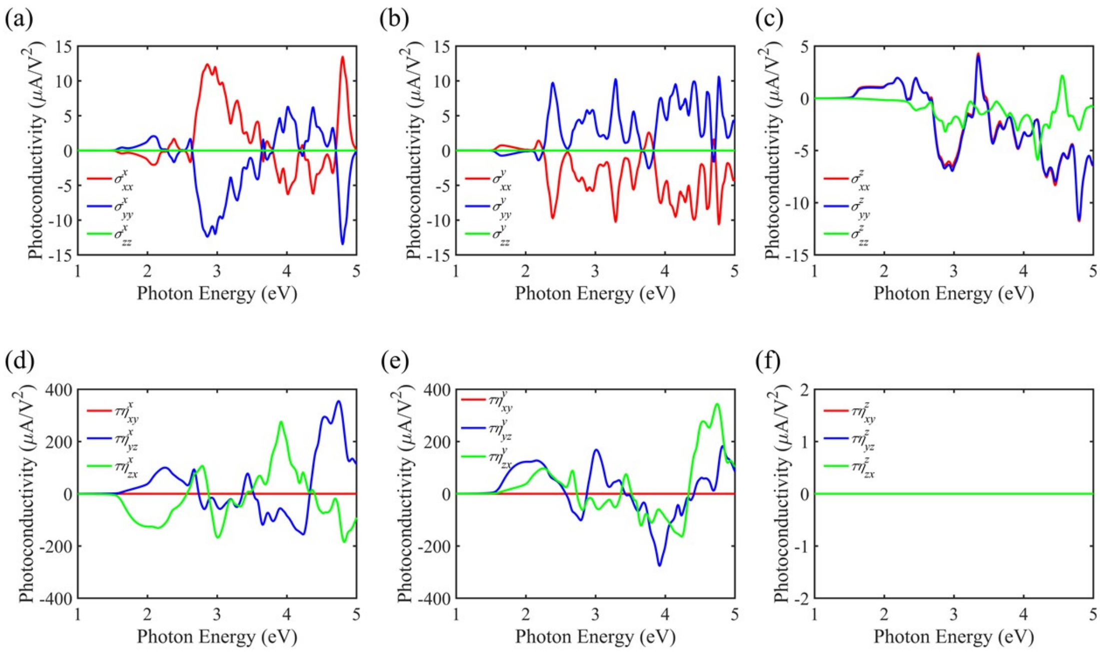

Figure S7. The SC and IC photoconductivities of CIPS in the FE2 phase.

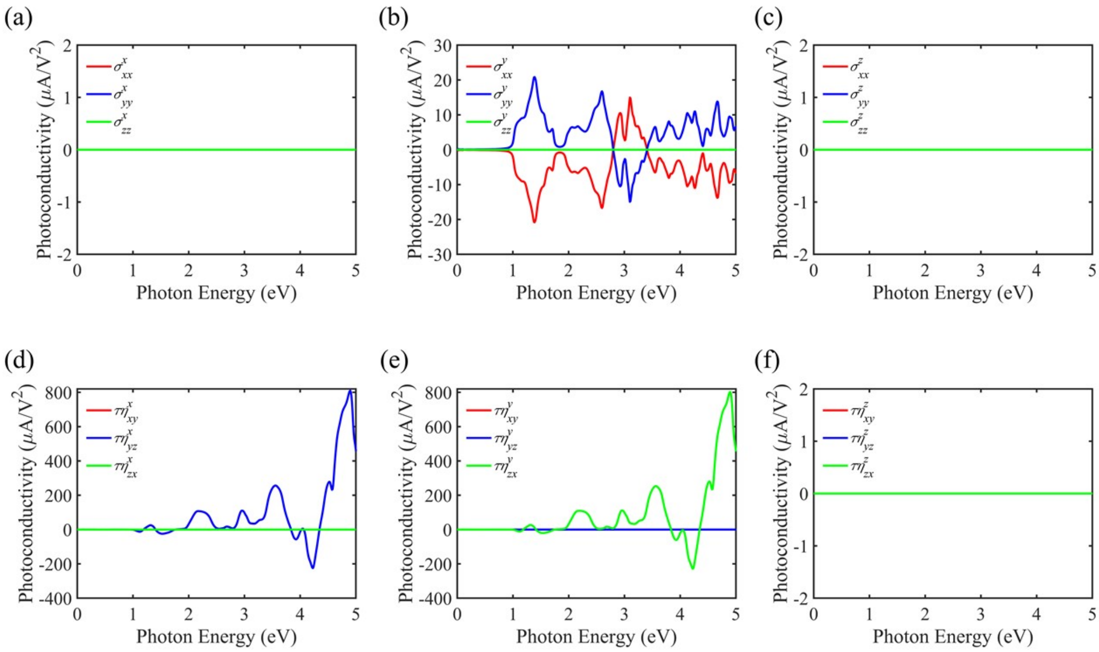

Figure S8. The SC and IC photoconductivities of CIPS in the PE phase.

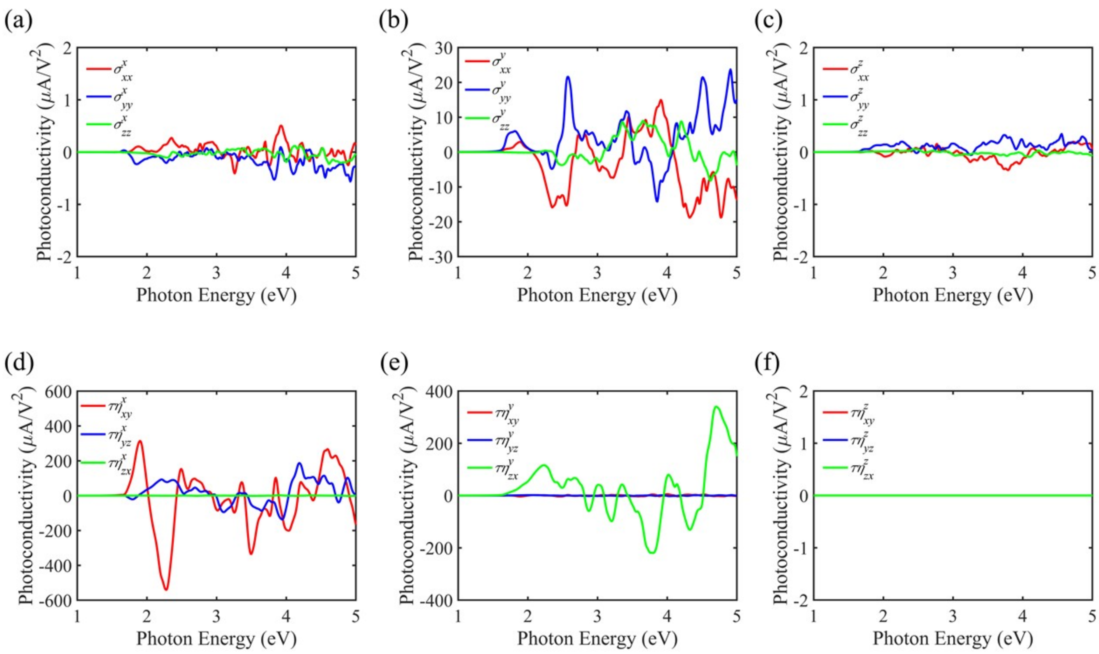

Figure S9. The SC and IC photoconductivities of CIPS in the AFE phase.

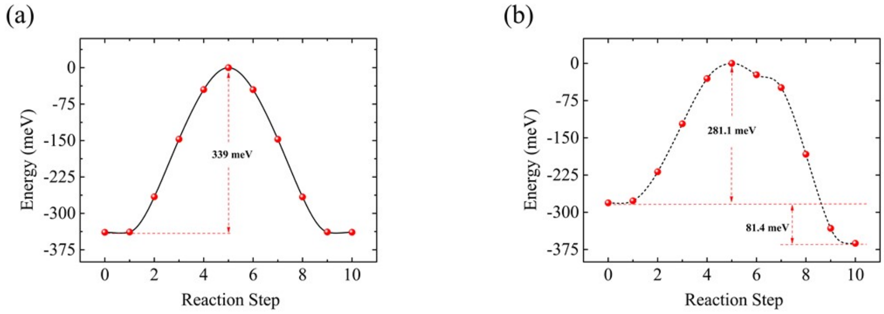

Figure S10. The CI-NEB path for the (a) FE1 to FE2 and (b) FE1 to AFE phase transition in CIPS.

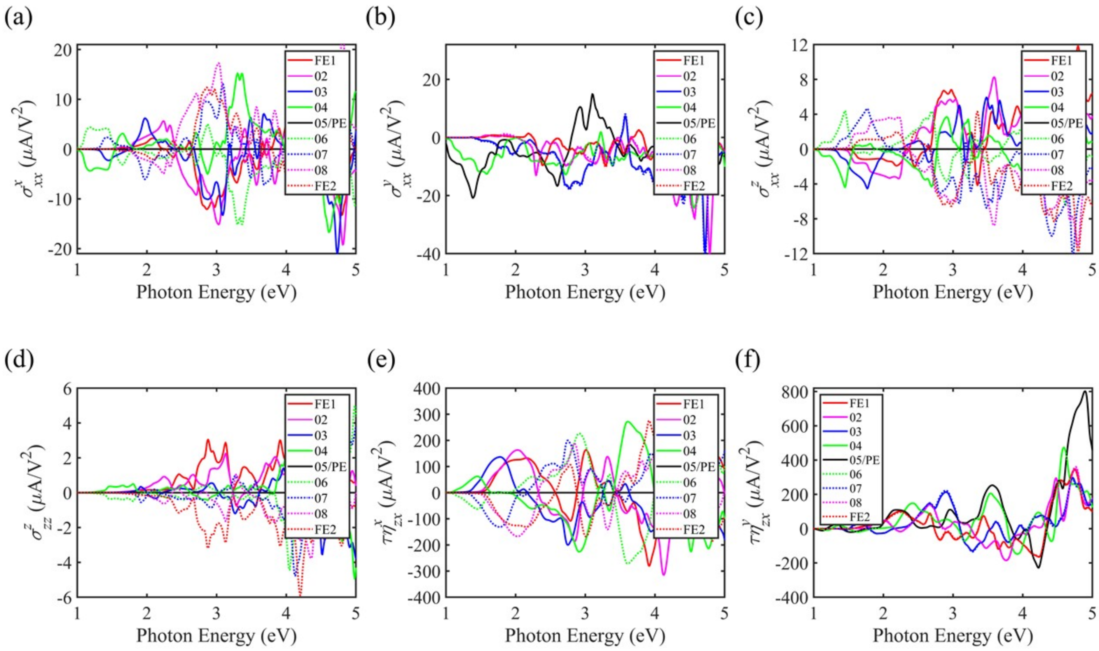

Figure S11. The evolution of photoconductivities during the FE1 to FE2 phase transition in CIPS.

(a) σ_{xx}^{x}. (b) σ_{xx}^{y}. (c) σ_{xx}^{z}. (d) σ_{zz}^{z}. (e) $\tau\eta_{zx}^{x}$. (f) $\tau\eta_{zx}^{y}$.

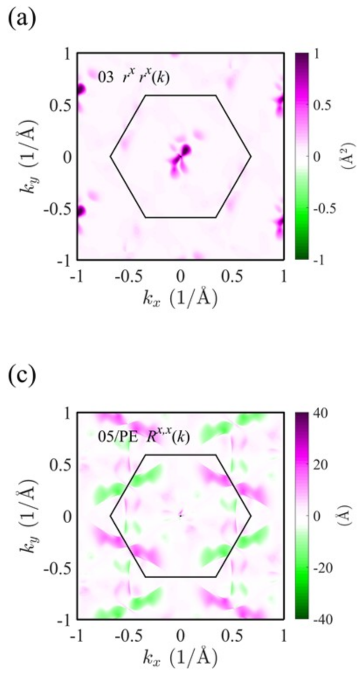

Figure S12. (a) and (b) the transition rate $r^x r^x(\boldsymbol{k})$ of σ^x_{xx} in the 03 and 07 structure. The (c) shift vector $R^{x,x}(\boldsymbol{k})$ and (d) transition rate $r^x r^x(\boldsymbol{k})$ of σ^x_{xx} in the 05/PE structure.

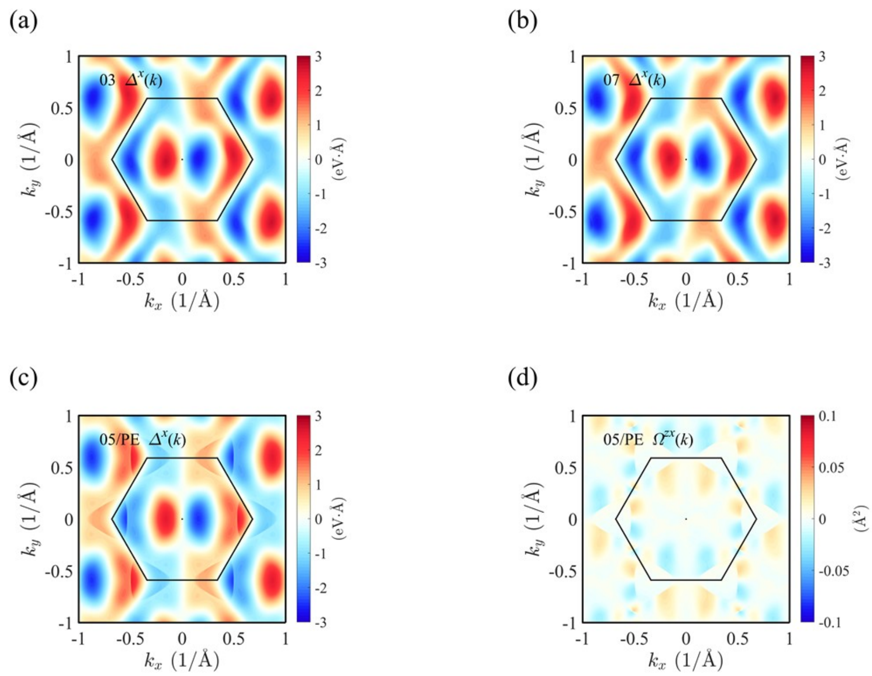

Figure S13. (a) and (b) the velocity difference $\Delta^x(\boldsymbol{k})$ of $\tau\eta^x_{zx}$ in the 03 and 07 structure. The (c) velocity difference $\Delta^x(\boldsymbol{k})$ and (d) Berry curvature $\Omega^{zx}(\boldsymbol{k})$ of $\tau\eta^x_{zx}$ in the 05/PE structure.

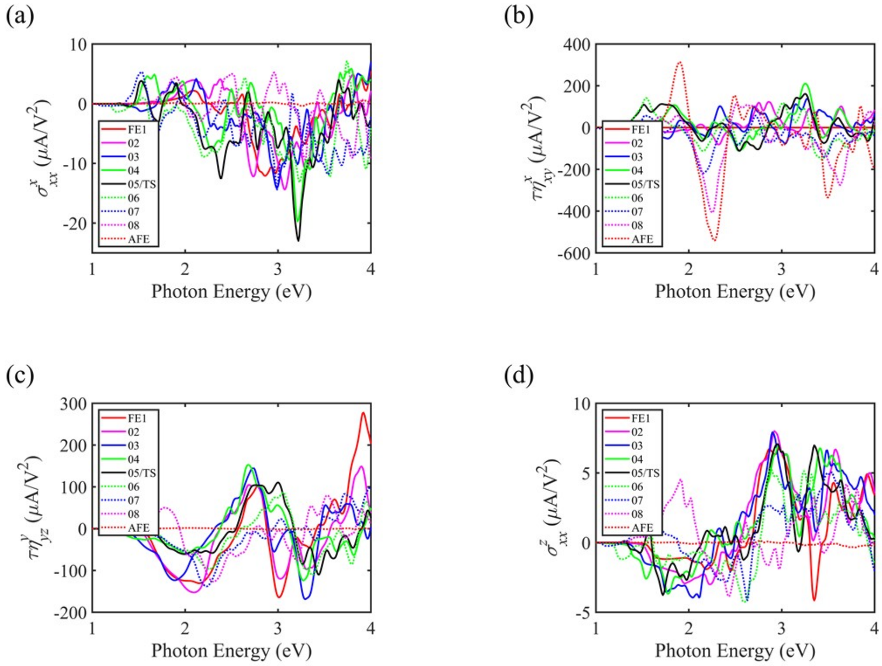

Figure S14. The evolution of photoconductivities during the FE1 to AFE phase transition in CIPS.

(a) σ_{xx}^{x}. (b) $\tau\eta_{xy}^{x}$. (c) $\tau\eta_{yz}^{y}$. (d) σ_{xx}^{z}.

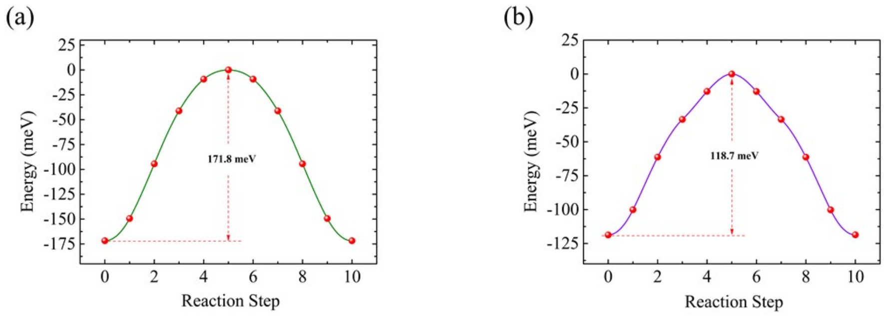

Figure S15. The CI-NEB path for the FE1 to FE2 phase transition in CIPSe (a) and CIPTe (b).

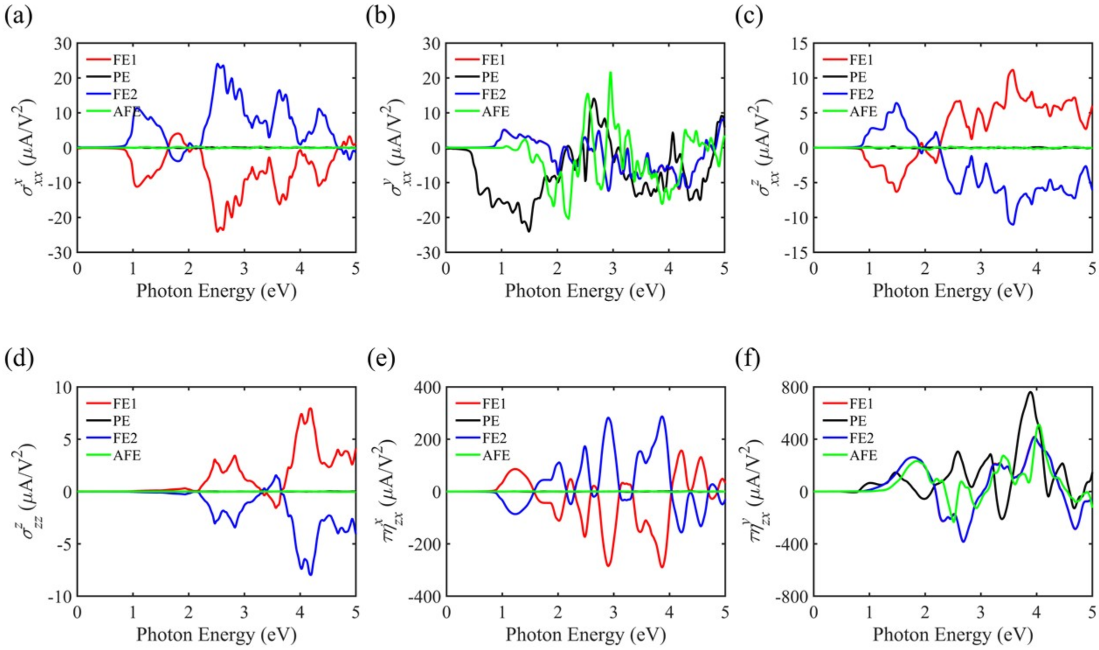

Figure S16. The SC and IC photoconductivities of CIPSe in the FE1, FE2, PE, and AFE phases.

(a) σ^x_{xx}. (b) σ^y_{xx}. (c) σ^z_{xx}. (d) σ^z_{zz}. (e) $\tau\eta^x_{zx}$. (f) $\tau\eta^y_{zx}$.

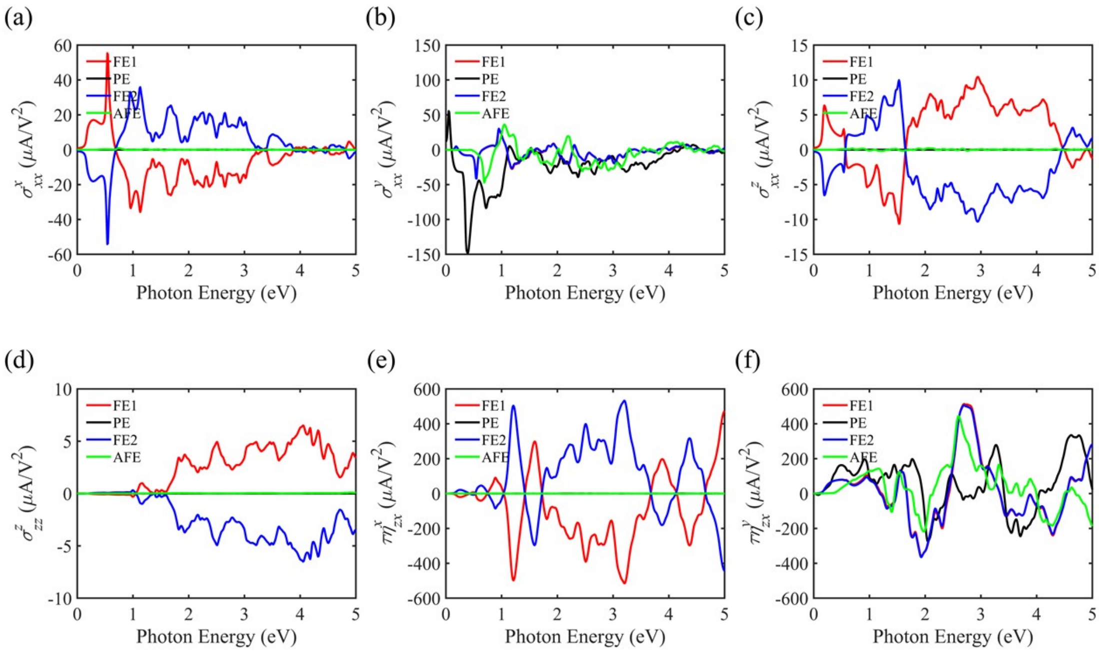

Figure S17. The SC and IC photoconductivities of CIPTe in the FE1, FE2, PE, and AFE phases.

(a) σ^x_{xx}. (b) σ^y_{xx}. (c) σ^z_{xx}. (d) σ^z_{zz}. (e) $\tau\eta^x_{zx}$. (f) $\tau\eta^y_{zx}$.

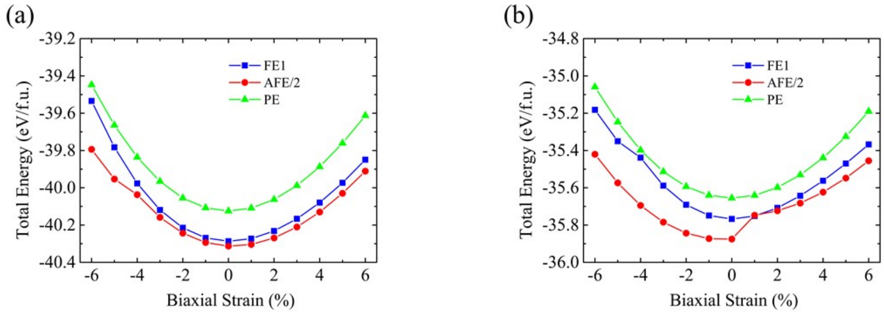

Figure S18. The relationship between the total energy and strain for the FE1, PE, and AFE phases of CIPSe (a) and CIPTe (b).

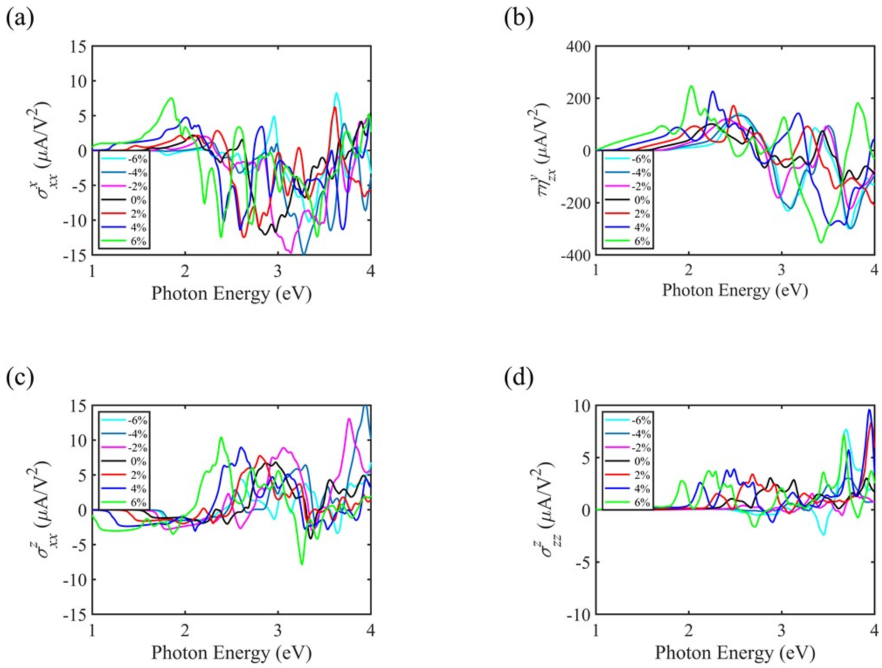

Figure S19. The SC and IC photoconductivities of CIPS in the FE1 phase under in-plane biaxial strain. (a) σ_{xx}^{x}. (b) $\tau\eta_{zx}^{y}$. (c) σ_{xx}^{z}. (d) σ_{zz}^{z}.

Supplementary references

(1) W. Kraut and R. von Baltz, *Phys. Rev. B*, 1979, **19**, 1548-1554.

(2) R. Von Baltz and W. Kraut, *Phys. Rev. B*, 1981, **23**, 5590-5596.

(3) J. E. Sipe and A. I. Shkrebtii, *Phys. Rev. B*, 2000, **61**, 5337-5352.

(4) D. E. Parker, T. Morimoto, J. Orenstein and J. E. Moore, *Phys. Rev. B*, 2019, **99**, 045121.

(5) H. Xu, H. Wang, J. Zhou and J. Li, *Nat. Commun.*, 2021, **12**, 4330.

(6) X. Mu, Y. Pan and J. Zhou, *npj Comput. Mater.*, 2021, **7**, 61.

(7) A. M. Cook, B. M. Fregoso, F. De Juan, S. Coh and J. E. Moore, *Nat. Commun.*, 2017, **8**, 14176.